Two high-yield complementary methods to sort cell populations by their 2D or 3D migration speed

Aditya Arora[a], Jorge Luis Galeano Niño[b], Myint Zu Myaing[a], Shumei Chia[c], Bakya Arasi[a], Andrea Ravasio[a,d], Ruby Yun-Ju Huang[e], Ramanuj Dasgupta[c], Maté Biro[c], and Virgile Viasnoff[a,f*]

[a]Mechanobiology Institute, National University of Singapore, Singapore 117411; [b]EMBL Australia, Single Molecule Science Node, School of Medical Sciences, University of New South Wales 2052, Sydney, Australia; [c]Laboratory of Precision Oncology and Cancer Evolution, Genome Institute of Singapore/A*STAR, Singapore 138632; [d]Pontificia Universidad Católica de Chile, Santiago, Chile; [e]Cancer Science Institute of Singapore, National University of Singapore, Centre for Translational Medicine, Singapore 117599; [f]Centre National de la Recherche Scientifique, BMC2, 5 A engineering drive 1, Singapore 1175411

ABSTRACT The potential to migrate is one of the most fundamental functions for various epithelial, mesenchymal, and immune cells. Image analysis of motile cell populations, both primary and cultured, typically reveals an intercellular variability in migration speeds. However, cell migration chromatography, the sorting of large populations of cells based on their migratory characteristics, cannot be easily performed. The lack of such methods has hindered our understanding of the direct correlation between the capacity to migrate and other cellular properties. Here, we report two novel, easily implementable and readily scalable methods to sort millions of live migratory cancer and immune cells based on their spontaneous migration in two-dimensional and three-dimensional microenvironments, respectively. Correlative downstream transcriptomic, molecular and functional tests reveal marked differences between the fast and slow subpopulations in patient-derived cancer cells. We further employ our method to reveal that sorting the most migratory cytotoxic T lymphocytes yields a pool of cells with enhanced cytotoxicity against cancer cells. This phenotypic assay opens new avenues for the precise characterization of the mechanisms underlying hither to unexplained heterogeneities in migratory phenotypes within a cell population, and for the targeted enrichment of the most potent migratory leukocytes in immunotherapies.

INTRODUCTION

Cell migration plays a pivotal role in all stages of the life of a multicellular organism. During development, cells migrate over long distances to give rise to tissue morphogenesis. Similarly, cell migration is crucial in wound healing for the supply of both progenitor cells and immune cells to the site of injury to enable regeneration and prevent infections, respectively. Further, aberrant migration of diseased cells such as cancer cells leads to their dissemination and thus, facilitates metastasis. As a result, a variety of methods have been developed to study the migration of cells. Migration driven by chemotaxis and transmigration is often tested using Boyden chambers (Chen, 2005), wherein migratory cells are allowed to migrate from one compartment into another through a porous membrane. Chemotactic gradients are created either by the addition of soluble factors or by culture of secretory cells in one of the compartments. Detection of transmigrated cells is usually achieved via spectrophotometry using a plate reader or via flow cytometry. Wound healing assays (also referred to as scratch assays) are preferentially used to study collective cell migration. They rely on creating a gap or a scratch in a two-dimensional (2D) monolayer of cells and to image the collective invasion of the freed space by the surrounding cells. Time-lapse imaging allows for basic measurements such as the speed of gap closure, often considered a quantitative proxy for cell migration propensity (Ashby and Zijlstra, 2012). Other quantitative

measurements can be performed such as the roughness of the migration front, indicative of the cohesion in the collective behavior of the cells. This type of assay is widely used as a simple first phenotypic characterization of cancer cells. Its simplicity and straightforward adaptability to quantitative high-resolution imaging makes it an assay of choice to understand the molecular basis of collective cell migration. Approaches to study cell migration in three dimensions (3D) are less popular due to the technical challenges of imaging. They often rely on the generation of spheroids in a matrix environment and allowing the cells to "sprout" off the initial cell cluster. Quantitative measurement of the number of sprouting cells and the mean distance traversed reveals the migration potential of the tested cell population (Kramer *et al.*, 2013).

Frequently, these assays reveal heterogeneity of migratory behavior within a cell population; however, the quantitative analysis usually provides only a migration index averaged over the entire cell population (Parker *et al.*, 2018). Despite the heterogeneity observed by imaging, these assays do not provide an easy (if any) means to sort and to retrieve cells within the population based on their migration behaviors. Single-cell transcriptomics now allows for quantitative assessment of the single-cell heterogeneity in cancer cell populations and can reveal the drift of subpopulations of cells with enhanced metastatic potential. It thus creates a need for phenotypic migration assays that can 1) sort cells based on migration potential, 2) easily retrieve the sorted cells in a large quantity (of the order of 1×10^6 cells), and 3) permit subsequent gene expression or molecular tests on the sorted live population. The isolation of such migratory cells facilitates the identification of invasion signatures that can then be used for prognosis or as therapeutic targets (Patsialou *et al.*, 2012). In addition, such an assay may be used to isolate cells with better motility for therapy such as in regenerative medicine and immunotherapy.

Very few such assays have been developed to date. When they exist, they are either of very low throughput, or difficult to implement or parallelize. One such method was developed by Lin *et al.*, where polyacrylamide microfluidic channels were employed to segregate cells based on their motility under a chemokine gradient, followed by protein expression analysis by in situ Western blotting (Lin *et al.*, 2018). In another work, the ability of migrating cells to phagocytose fluorescent particles from a substrate was used to study and sort cells using fluorescence-activated cell sorting (FACS; Windler-Hart *et al.*, 2005). Taken together, these and some other methods (Jeong *et al.*, 2011; Bajpai *et al.*, 2014; Chen *et al.*, 2015; Yankaskas *et al.*, 2019) provide a tool for 2D motility-based sorting using complex micropatterns, microfluidic devices, or FACS-based methods. However, due to the involvement of these high-end technologies, the use of such methods is limited by their cost, complexity, and scalability.

Further, there is a dearth of methods that can be used to sort cells based on their ability to migrate in 3D microenvironments. While 2D motility studies have provided significant insight into basic biological processes, their use is still limited by the fact that most physiological cell migration occurs in 3D microenvironments (Kramer *et al.*, 2013). Wyckoff *et al.* used matrigel and growth factor–loaded microneedles to capture migratory cells from tumors in living rats (Wyckoff *et al.*, 2000). This technique was later used to perform gene expression and molecular analysis of a small number of cells to identify novel invasive signatures (Wang *et al.*, 2002, 2003, 2004). However, this method is limited by its use in larger in vivo tumors only. Moreover, certain cell types, such as leukocytes, expand in suspension culture and exhibit characteristic migration behavior only in 3D extracellular matrix microenvironments. Thus, for such cell types, and in order to render the process more physiological, there is also a need to develop methods for in vitro 3D motility-based cell sorting.

Here we propose readily implementable methods to separate a faster migrating subpopulation of cells from a heterogeneous population based on migration in 2D or 3D environments. The 2D migratory sorting relies on a layered-polydimethyl siloxane (PDMS) microwell device, which was demonstrated to be useful for separating a heterogeneous cancer cell population into a more homogenous population based on migration. The 3D sorting utilizes hierarchical hydrogel systems consisting of collagen microgels suspended in degradable bulk hydrogel. This method can not only separate cancer cells in 3D but can also be used for more challenging cell types such as primary leukocytes (here cytotoxic T lymphocytes; CTLs). We also characterize the sorted populations in terms of their epithelial–mesenchymal transition (EMT) status, receptor clustering, transcriptomic data, or cytotoxic function depending on the cell type.

RESULTS

The 2D and 3D sorting approaches are parallel small-scale extensions of the wound healing assays performed on imbricated substrates that can be isolated individually by macroscopic manipulations. Initially, groups of unsorted cells are locally confined in a series of scattered predefined regions. The cells are then allowed to spontaneously migrate away from the original confinement zone onto (into) another substrate. In the 2D case the surrounding substrate is mechanically detached from the initial confinement zones, whereas, in the 3D case the separation is performed by selective matrix digestion. Cells are thus sorted by the physical separation of the pre- and postmigration substrates.

Fabrication of the 2D sorting device

An extensive description of the device is detailed in *Materials and Methods* and exemplified in Figure 1 and Supplemental Movie 1. Briefly, the 2D migration sorting assay (2D-MSA) comprises three layers of PDMS sheets laminated together: a protective layer at the top, a middle collection layer, and finally a spacing layer. Arrays of holes (300–500 µm in diameter) are then perforated across the three-layer substrate using a commercial laser cutter. The system is then assembled on a base PDMS layer. We then seeded cells on the substrate at 70–80% confluency. Cells fall into the cavities/microwells and adhere after ~30 min, and subsequently the protective layer is removed using lab forceps after rinsing the substrate. Cells are then allowed to migrate up the cavity walls until they reach the collection layer that was initially devoid of any cells. After 1 to 3 d, the layers are individually peeled off with tweezers. The collection layer is enriched with fast migrating cells while the base layer is enriched in slow migrating cells. Cells can be trypsinized immediately from the layer, leading to a collection of around 300–500 cells per microwell on the collection layer. Alternatively, cells can be left to expand on the separated layer yielding around 2000–4000 cells per well. The diameter of the cavities was optimized to ensure that cells initially located in the center of the well could still migrate away from the confinement zone within the migration period of 1–3 d. The thickness of the protective layer was not important. However, 250-µm-thick collection layers offered sufficient mechanical stability to be peeled easily at a later stage with simple tweezers. We varied the thickness of the spacing layers to tune the sorting capability of the device. The spacing between the cavities is a compromise. We set it small enough to ensure a large density of wells, hence maximizing the total number of sorted cells. It is also large enough to preclude any cross-migration between cavities. Cell density can be varied based on the cell type. We practically implemented the assay in a six-well plate that
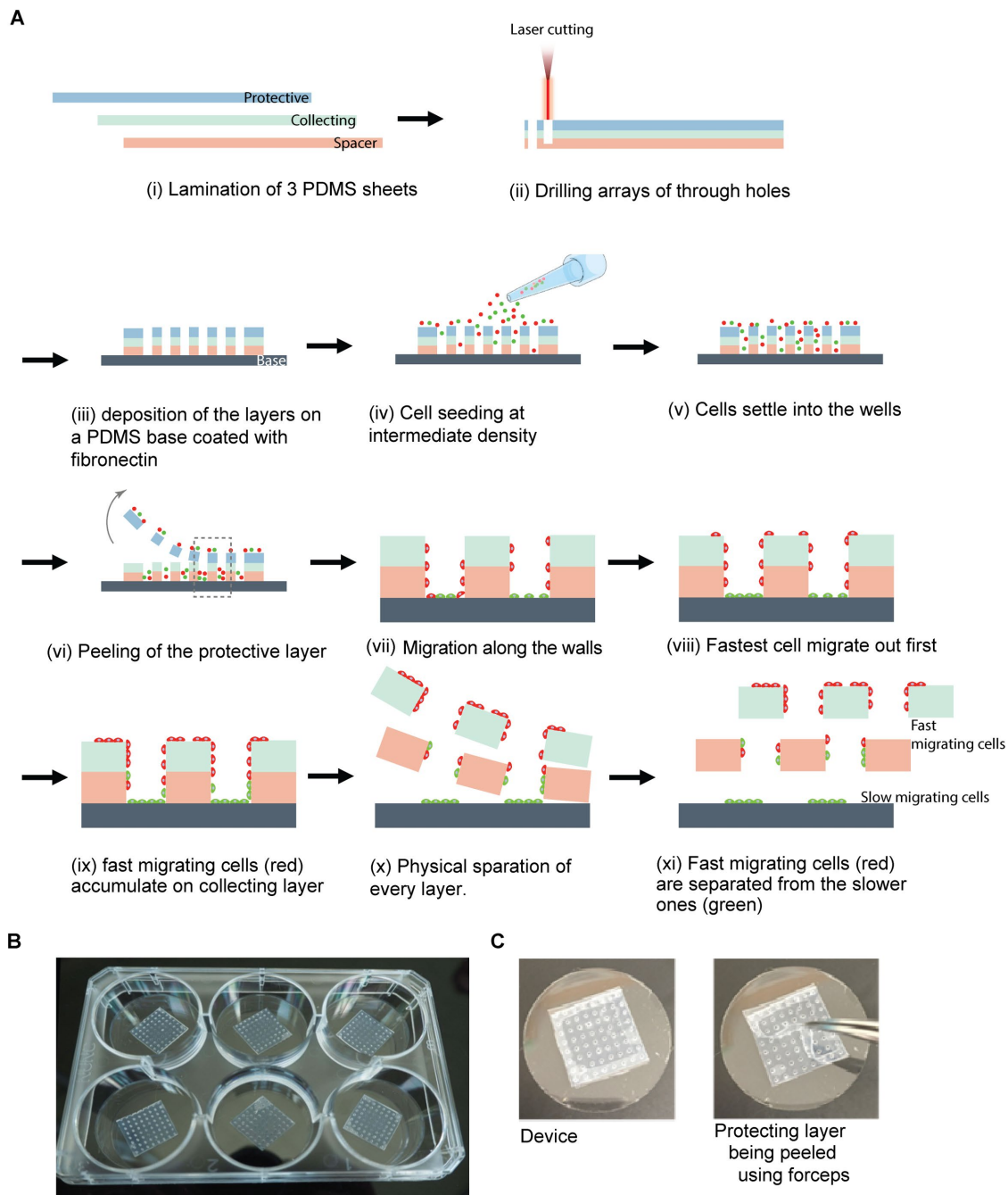
FIGURE 1: Layered-PDMS microwells for 2D migratory sorting of cells. (A) Schematic depicting the process of fabrication of a PDMS microwell-based device and its use for migratory sorting of cells. (B) Macroscopic image of the microwell-based devices in a six-well format. (C) Close-up of the final ready-to-use device, and the protecting layer being peeled off using forceps.

usually contains 64 such microwells per well, thus making the total migratory cell yield from the plate of the order of 1×10^6 cells.

Motility-based sorting of cancer cell lines

We first tested the sorting capabilities of the device using a 1:1 mix of two standard breast cancer lines (MCF7 and MDA MB 231) with distinct motility characteristics. MCF 7 cells are more epithelial-like and migrate collectively, whereas MDA MB 231 cells are mesenchymal-like with extensive migratory propensity (Lundgren *et al.*, 2009). We used cell tracker dyes to distinguish each population. The cells were seeded onto the devices coated with fibronectin. We used a

spacer thickness of 500 µm. Three days post seeding, some cells reached the collection layer of the device. Including the thickness of this layer, it corresponded to a migration of >750 µm. Using spectral imaging (Figure 2, A and B) we established that the population of cells on the collection layer at day 3 was approximately three times more enriched for MDA MB 231 cells as compared with initial seeding (Figure 2B; *N* = 12 wells from four batches). However, the bottom collecting layer shows only marginal enrichment of the less migratory MCF 7 cells, indicating that our method is more efficient to extract the fast migrating cells than the slow ones. We further evaluated the influence of spacer thickness on the sorting process,
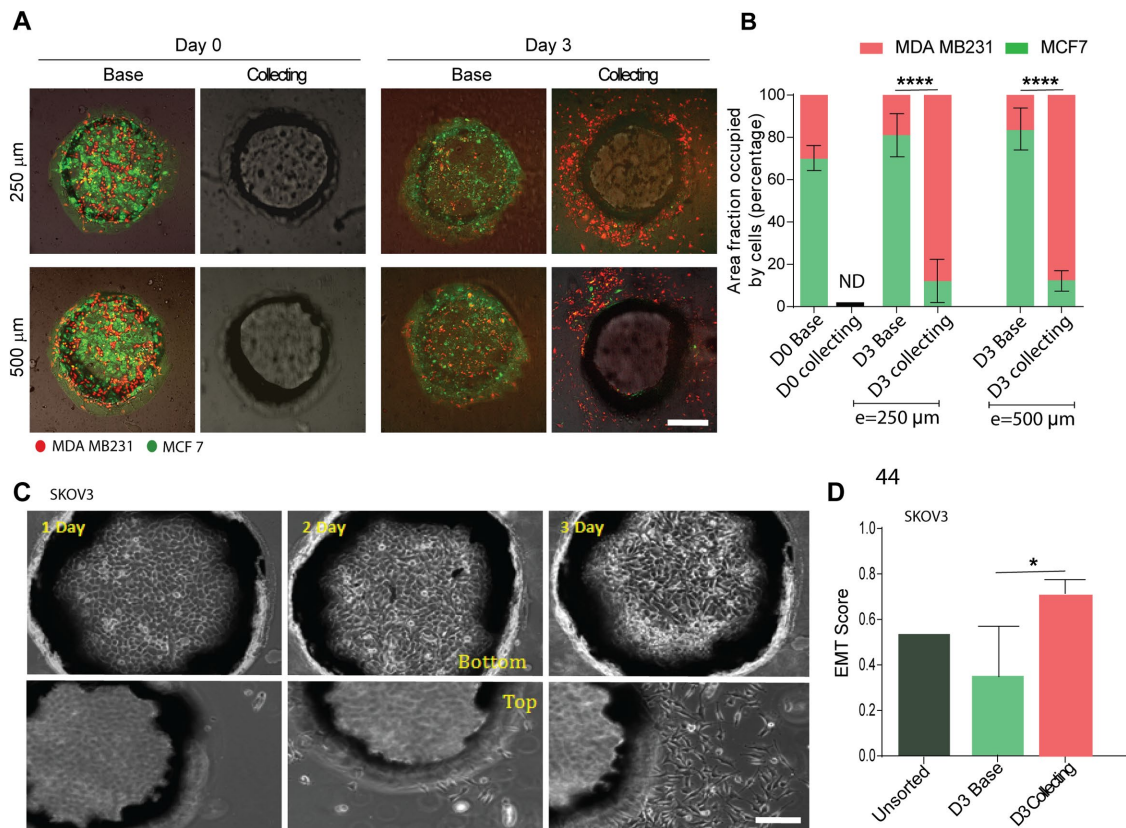
FIGURE 2: 2D migratory sorting of cells with varying migratory abilities and degree of epithelial to mesenchymal transition (EMT) state. (A) Fluorescent images of bottom and top regions of microwells with MDA MB 231 (red) and MCF-7 (green) cells in microwells with different spacer height on day 1 and after 3 d of incubation (scale bar: 200 μm). (B) Quantification of area fraction occupied by MDA MB 231 and MCF 7A cells on top and bottom layers before and after migration (N = 12 microwells from four biological replicates). (C) Phase contrast images of SKOV3 cells migrating out of microwells at days 1, 2, and 3 after seeding (scale bar: 100 μm). (D) Quantification of EMT score based on expression of a panel of genes (ref) for cells isolated from the top and bottom layers; secondary x-axis depicts the EMT score of the unsorted SKOV3 cells (N = 3). *, <0.05; ****, <0.0001 by Student's t test.

for which we used spacers of thickness 250 and 500 μm. As expected, significantly more cells (p < 0.01) migrated out onto the collection layer in the device with a 250-μm spacer thickness (Supplemental Figure 1; N = 12 wells from four batches). However, no significant differences were observed in terms of efficiency of sorting between the two spacer thicknesses (Figure 1B). Therefore, henceforth we employed a spacer thickness of 250 μm for all experiments.

Thereafter, we tested if cancer cell lines presenting an intrinsic variability linked to genome instability can be sorted based on migration speed. We used the ovarian cancer cell line SKOV3. This cell line is reported to be intermediate between epithelial and mesenchymal (with a reported epithelial to mesenchymal transition score of 0.38; Tan *et al.*, 2014) and with heterogeneous cell subpopulations showing distinct migratory and invasive capacities (Bai *et al.*, 2015). Following similar sorting conditions (250-μm spacer), spindle-shaped cells accumulated by day 2 on the collecting layer (Figure 2C). We harvested enough cells by day 3 in order to subsequently perform standard RT-qPCR to compute the EMT score of the most and least migratory populations according to Tan *et al.* (Tan *et al.*, 2014). We found that cells on the collecting layer had a significantly higher (p < 0.05) EMT score (0.71) compared with cells on the base of the device (0.35) (Figure 2D; N = 3 batches). It confirmed that the method was not only able to sort cells with large EMT score difference, that is, MCF-7 (−0.35) and MDA MB 231

(0.44) but sensitive enough to separate cells with differential migration ability from a single heterogeneous population with a small difference in their EMT scores. Further, the sorting method directly provided enough cells to harvest 2–5 μg RNA to perform standard RT-qPCR.

Motility-based sorting of metastatic cells and correlation with ephrin clustering and transcriptomics

We then posited that the phenotypic selection of a migratory cell subpopulation would also be reflected in their transcriptomic profile. We thus tested the approach using a patient-derived head and neck cancer primary cell line (PDC) isolated from patients' lymph node metastatic lesions (HN120M; Chia *et al.*, 2017; Sharma *et al.*, 2018). To obtain enough sorted cells for transcriptomics we compared two strategies: collecting sorted cells after 5 d of migrations (HN120M-S5d-E0d-top) or collecting cells after 3 d of migrations and expanding them separately for an additional 2 d (HN120M-S3d-E2d-top; Supplemental Figure 2A). For either method, three devices were enough to provide sufficient quantity and quality of RNA for transcriptomic analysis. We performed full transcriptomic analysis of the different cell populations (migratory vs. nonmigratory). As shown in Figure 3, A and B, we observed a sequential increase in the number of genes that are up-regulated in the migratory population (compared with nonmigratory population at the bottom layer) between D3 and D5. While ~307 genes were up-regulated in
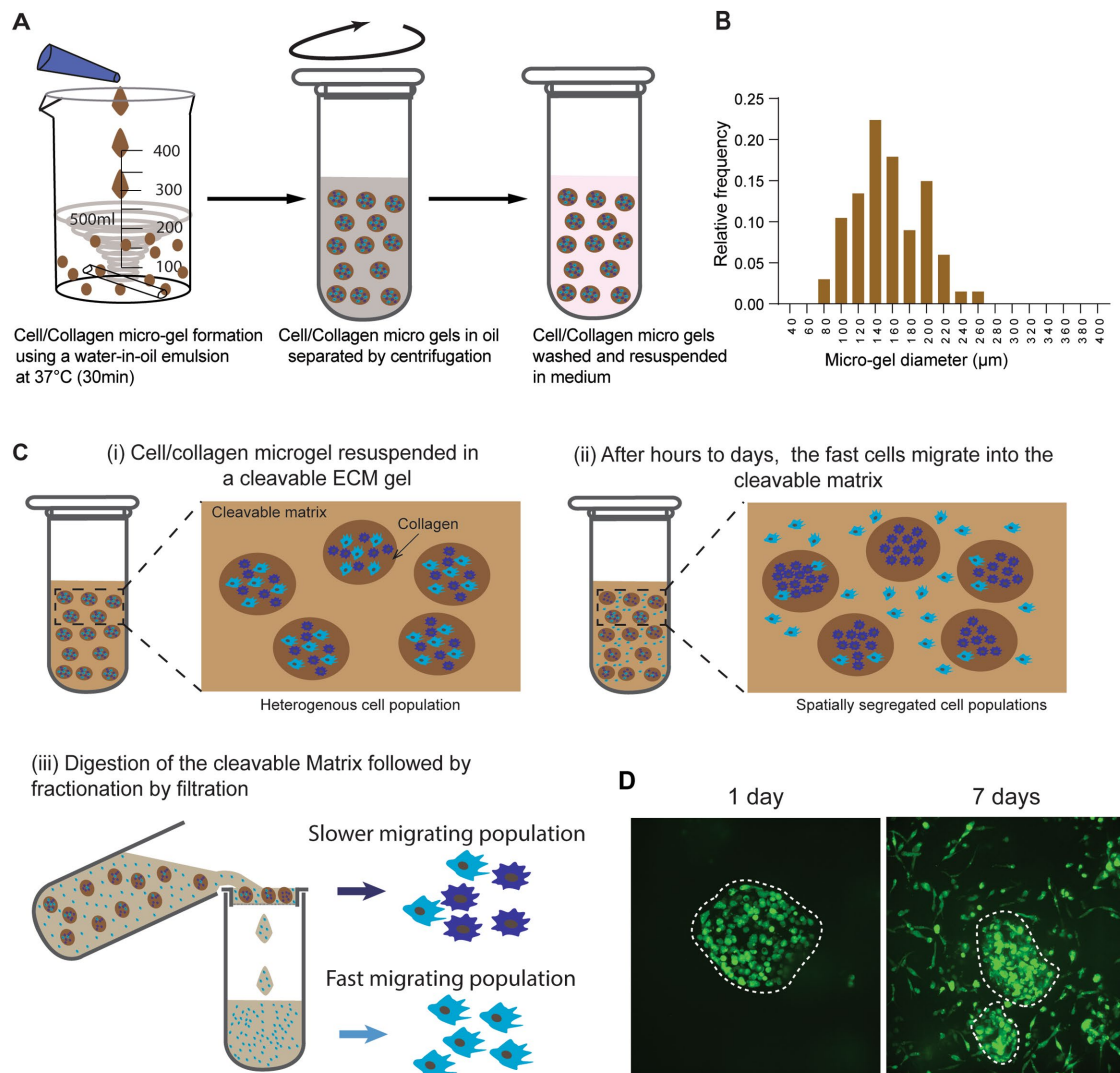
FIGURE 3: Analysis of genes that are up-regulated in the migratory populations. (A) Number of differentially up-regulated genes with log2-fold greater than 1 and *p* value less than 0.05 were used as inputs for Metascape using multiple gene list options with standard parameters (Zhou *et al.*, 2019). (B) The circus plot shows the overlap among gene lists. The outer arc represents the input gene list, while a dark-orange color on the inner arc represents the parts of the gene list that are also found in other lists. A light-orange color on the inner arc represents genes that are unique to the list. Purple lines link genes that are shared across lists. Blue lines link genes sharing the same ontology terms. (C) Heatmap of enriched GO terms for differentially up-regulated genes on day 3 and day 5, across replicates. Gray color represents the lack of significance, while the color scale indicates statistical significance. (D) Network layout of representative GO terms. Each circular node represents a single GO term. The size of the node corresponds to the number of input genes and color depicts its identity as shown in the legend. Thickness of the lines corresponds to the degree of similarity between nodes. (E) Molecular complex detection (MCODE) algorithm identifies clusters of interacting proteins among the input gene list. Color corresponds to the MCODE identity shown in the legend. (F) The pie sector represents the identity of samples containing the gene of interest.

FIGURE 4: Sorting of cells based on migration through a 3D hierarchical hydrogel system. (A) Schematic depicting the process for fabrication of cell-laden collagen microgels using water-in-oil emulsion. (B) Size distribution bar graph for cell-laden collagen microgels ($N = 70$). (C) Schematic depicting migratory sorting of cells based on differential migration through collagen microgels into outer hydrogel matrix. (D) Fluorescent images of MDA MB 231–GFP cell-laden microgels further embedded in HA-collagen hydrogels post 1 and 7 d of incubation.

D3, the D5 migratory cells displayed an approximately fivefold increase in the number of up-regulated genes (~1619). The genes that displayed increased expression in D3 were a subset of the differentially up-regulated genes in D5 and/or appeared to be highly related based on their molecular functions/gene ontology (GO) terms (as depicted in the chord diagrams in Figure 3B). Interestingly, while the D3 transcriptome appeared to be metastable, the D5 transcriptome of the migratory cells was found to be stable and reproducible among experimental replicates (Figure 3C). Altogether the gene expression analysis suggested a gradual change in the transcriptome of the migratory cells captured between D3 and D5. Importantly, pathway interactome analysis of the nature of the up-regulated genes suggested their function in promoting the migratory phenotype observed (including genes involved in wound healing), regulation of cell adhesion, ECM regulators (including those involved in ECM organization), Type 1 hemidesmosome assembly (critical in cell–substratum adhesion and a key regulator of cell migration), and cytokine-mediated signaling pathways among others (Figure 3D and Supplemental Figure 3, A and B). Importantly,

protein–protein-interaction network analysis suggested that the genes up-regulated in the migratory cells represent molecular modules with shared functions (Figure 3, E and F, and Supplemental Figure 3, C and D) that collaborate and contribute toward the migratory phenotype. Moreover, among the top 10 up-regulated genes in HN120M-S5d-E0d-top and HN120M-S3d-E2d-top, expression of the four genes (CEACAM6, CRYAB, SPRR3, and PGLYRP) that were conserved in the top 10 of at least two groups have previously shown a clear correlation with poor prognosis in different cancers, which further strengthens our results with respect to their relevance to progression of disease (Jantscheff *et al.*, 2003; Cho *et al.*, 2010; Qin *et al.*, 2014; Krochmal *et al.*, 2019).

In contrast to the number of up-regulated genes, the number of down-regulated genes was fairly consistent on both D3 and D5 (Supplemental Figure 4A), and across replicates (Supplemental Figure 4B). Notably, pathway analysis of these differentially expressed down-regulated genes suggested their function in the regulation of cell–cell junctions among others (Supplemental Figure 4, C–F). It is conceivable that these junctional proteins were
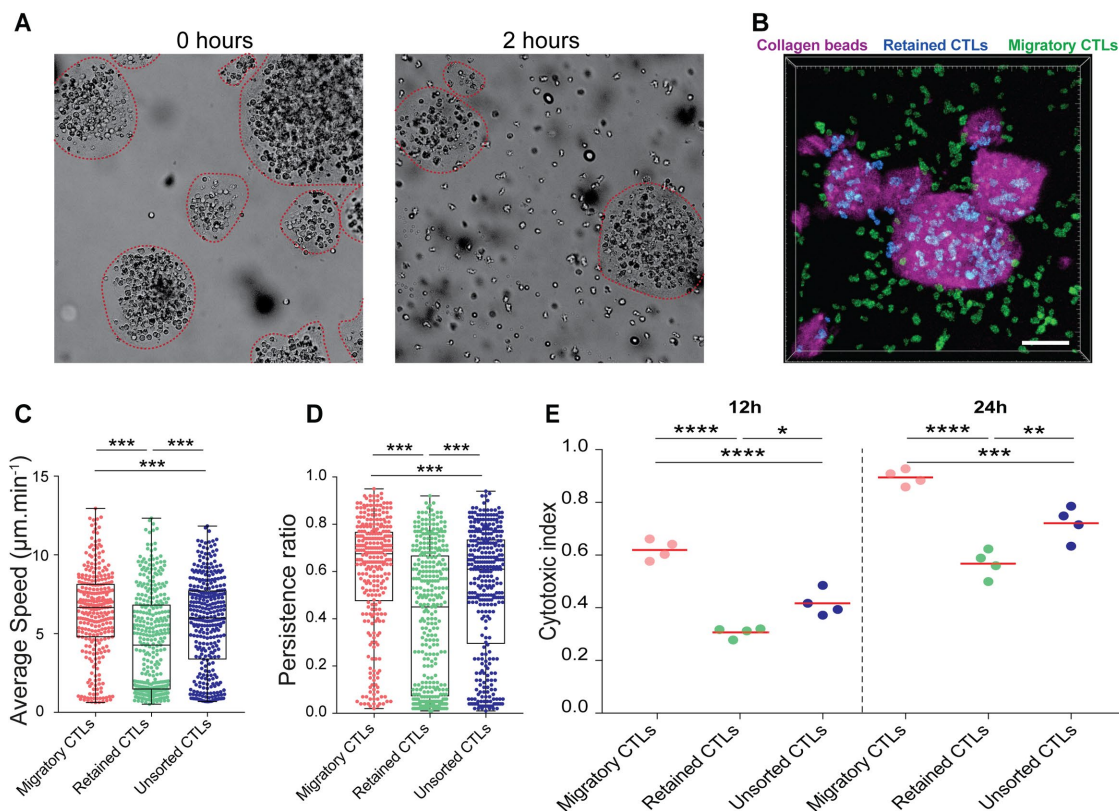
FIGURE 5: Migratory sorting and cytotoxic function of sorted T-cells. (A) Brightfield images showing CTLs embedded in collagen beads before and after 2-h incubation in TCM. (B) Confocal 3D image showing collagen beads (magenta) containing CTLs cultured for 2 h in TCM under regular conditions. Using image analysis, two T-cell populations were identified: the CTLs that were retained in the collagen beads (blue cells) and the ones that migrated out (green cells). (C) Distribution of the average speed of migratory, retained, or unsorted CTLs in 3D collagen matrices. Data points indicate individual tracks; box-whiskers: medians and quartiles from pooled data of three independent experiments; ***, $p < 0.001$ by Kruskal-Wallis test followed by Dunn's multiple comparison test. (D) Distribution of the persistence ratio of migratory, retained, or unsorted CTLs in 3D collagen matrices. Data points indicate individual tracks; box-whiskers: medians and quartiles from pooled data of four independent experiments; ***, $p < 0.001$ by Kruskal-Wallis test followed by Dunn's multiple comparison test. (E) Flow cytometry quantification of the cytotoxic index of migratory, retained, or unsorted CTLs after 12 or 24 h of incubation with target cells as indicated. Red bars indicate the mean of four independent experiments. *, $p < 0.05$; **, $p < 0.01$, and ****, $p < 0.0001$ by one-way ANOVA followed by Tukey's multiple comparison test.

down-regulated to facilitate the process of cell migration. The transcriptomic analysis suggests that the phenotypic sorting of these cells using this methodology can indeed successfully segregate cells based on their inherent differences in molecular/gene expression signatures.

Taken together, these experiments demonstrated that the cells accumulating atop the collecting layers presented phenotypic differences that indicate bona fide sorting based on migration speed within a heterogeneous population.

To further profile heterogeneity distribution of these populations at the single-cell level before and after sorting, we employed a phenotypic assay to quantify ephrin A (EphA) receptor activation at the single-cell level. The EphA score, which is a measure of such clustering, has been reported to correlate well with migration potential and to be relevant to describe heterogeneity in cells by providing EphA score distribution for a population (Ravasio *et al.*, 2019). Supplemental Figure 2B shows that cells collected from the base layer had EphA scores that were significantly lower ($p < 0.001$) than those obtained from the migratory cells after 3 d of cell migration (HN120M-S3d-E2d-top). Additionally, the distribution for the unsorted cells lies between the base and collecting layer cells. This

result also corroborates with a previous report that showed a strong correlation between EphA2 expression and cell motility in glioblastoma cells (Lin *et al.*, 2018). These results demonstrate that this is an effective method to enrich migratory subpopulations of cells that show significantly altered phenotype as compared with the parent population.

Motility-based sorting of cancer cells in 3D hierarchical hydrogels

We then extended the concept of entangled dissociable substrates to 3D migration. We devised the composite substrate described in *Materials and Methods* and Figure 4. Briefly, we first created collagen microbeads embedding cells using an emulsion in mineral oil at 37°C (Figure 5A). A majority of these microbeads were in the range of 100–200 µm in diameter, with the average size being 155 ± 38 µm (Figure 5B and Supplemental Figure 4A). The collagen microbeads are collected by gentle centrifugation, then washed and resuspended in growth medium. The microbeads are then dispersed in an enzymatically degradable hyaluronic acid (HA) hydrogel mixed with very low concentration of collagen to aid cell migration (Jeong *et al.*, 2011). The surrounding matrix is rapidly cross-linked (<1 min)

while mixing to minimize the sedimentation of the collagen beads. The cells are allowed to migrate from the collagen microbeads into the surrounding cleavable matrix for 7 d (Figure 4, C and D). The cleavable matrix is then selectively digested using hyaluronidase enzyme for 3 h until it is solubilized to release all the migrated cells. The suspension is then filtered using a cell strainer (40 μm) to separate the collagen beads containing the less mobile cells from the surrounding medium containing the most migratory cells. Each fraction can then be cultured and expanded separately. It is straightforward to scale the methods increasing the number of droplets and the volume of the assay. Starting with typically 1×10^6 cells, we used a set of five, 100-μl gels, leading to a final retrieval of ~$(2-4) \times 10^5$ sorted cells.

We first validated the approach by testing the migration of MDA MB 231 cells from the collagen beads into the outer HA hydrogel. After 7 d of culture (Figure 5D) a large population of elongated MDA MB 231 cells was able to move across the interface of two matrices and had migrated out into the outer HA hydrogel validating the capacity of these cells to migrate out of the initial gel. We then used a 1:1 mixture of MCF7:MDA MB 231 cells. After 7 d the population of cells in the microbead remains similar to the initial unsorted population; however, the cells extracted from the surrounding HA matrix was predominantly (>95%) MDA MB231 type (Supplemental Figure 4, B–D). Although the separation time was longer than in 2D for cancer cells, the 3D method appeared even more relevant to separate cells hardly migrating in 2D but with extensive amoeboid 3D migratory capability such as T-cells (Friedl *et al.*, 1998).

Motility-based sorting of T-cells and correlation with their cytotoxic potential

We used primary mouse Lifeact-EGFP cytotoxic CD8^{+} T-cells (CTLs; Niño *et al.*, 2020) isolated from OT-1× Lifeact-EGFP mice spleens. CTLs were embedded in the collagen microbeads as described in *Materials and Methods*. As CTLs migrate much more rapidly than cancer cells in 3D and can reach speeds up to 12 μm/min in collagen matrices (Galeano Niño *et al.*, 2016), the experimental timeline was markedly reduced to hours and we could simply resuspend the collagen beads in cell culture medium and forgo the surrounding HA hydrogel that otherwise sustains migrating cells for days. Within 2 h, about half of the cells had migrated from the collagen beads into the outer medium (Figure 6, A and B). We sieved the cells suspended in the medium from the collagen beads (see *Materials and Methods*). We then measured the average migratory speed of the individual T-cells from the sorted and unsorted population fractions (Supplemental movies 2 and 3). To this end we embedded each cell population in a collagen matrix and employed quantitative image analysis–based tracking of single cells as previously described (Niño *et al.*, 2020; Figure 5C). This revealed a clear enrichment of the fast migrating (average speed = 6.31 ± 2.8 μm/min) CTLs in the population isolated from the surrounding medium. By contrast, the population that remained in the microbeads was less migratory (average speed = 4.44 ± 3.12 μm/min). The speed distribution of unsorted cells was intermediate between the two subpopulations (average speed = 5.65 ± 2.9 μm/min). Interestingly, the more migratory cell fraction also migrated more directionally (Figure 5D) as indicated by a higher ratio of net displacement over total path length, referred to as persistence ratio (see *Materials and Methods*).

We finally tested if the sorted CTL populations were also functionally distinct, that is, if they displayed substantially different killing efficiency. To this end, we mixed the CTLs with fluorescently labeled cognate (+SIINFEKL) and noncognate (−SIINFEKL) EL4 tumor cells

(ATCC: TIB-39) at a ratio of 1:4:4. We used flow cytometry to determine the ratio between live target and nontarget cells after 12 and 24 h of coincubation. The cognate and noncognate cells were differentially labeled and thus could be counted using flow cytometry analysis. Using FACS, we quantified the ratio of target to nontarget cells excluding the amount of killed cells (positive to DAPI). This ratio was compared with control conditions when the cancer cells were not exposed to T-cells. We used this quantification as the cytotoxic index monitoring the killing potential of T-cells (Figure 5E).

The faster migrating T-cells showed an unambiguous 2- and 1.6-fold increase in killing efficiency as compared with slow migratory and unsorted cells, respectively ($N = 10^4$ cells; Figure 5E). Of note is the fact that the large excess of cancer cells is a standard way to ensure that killing efficiency is not limited by the ability of a CTL to encounter a cognate cell and hence is physically not favored by enhanced motility. In these conditions the functional correlation must stem from associated activations of molecular pathways that are at play for both migration and killing. Activation of the cytoskeleton is likely to play a role in both processes.

These results suggest that such a method could potentially be used in the context of immunotherapeutic applications to enhance the killing efficiency of adoptively transferred cells.

DISCUSSION

Overall, we have established a method to sort cells (cell lines, PDCs, and primary CTLs) based on their 2D and 3D spontaneous migration characteristics. We demonstrated how such a phenotypic assay can be then coupled to transcriptomic or functional characterization of the sorted cells. The direct sorting does not involve selection based on any marker and directly tests the migration property. Moreover, as demonstrated, both the 2D and 3D methods are scalable to give cell (≈10^6 cells)/RNA (2–5 μg) yield that is sufficient to perform downstream assays such as RT-qPCR, imaging, transcriptomics, and FACS. Therefore, the method is also likely to be a beneficial tool for functional proteomics studies because very few approaches allow such discrimination.

Besides optical characterization, few tools exist that can phenotypically sort cells based on migration speed. Table 1 outlines a comparison of previously reported methods for migratory sorting with the current work. Previous migration chromatography approaches are often limited by the complexity or the low yield of the devices that preclude subsequent testing of the sorted populations. For example, Chen *et al.* designed a microfluidic migration platform that can be used to profile chemotactic heterogeneity in cells at a single-cell resolution. The migration in their work is, however, strictly driven by chemokine gradient and the process can yield only a limited number of cells (tens of cells) per experiment (Chen *et al.*, 2015). In another method, phagocytosed fluorescent particles coated on the substrate are used as a measure of cell migration; this can be later concatenated with FACS to separate cells with different migration rates (Windler-Hart *et al.*, 2005). While this method provides excellent single-cell resolution in terms of describing the migration ability of cells, the downstream analysis results may be significantly clouded by the presence of internalized particles. It is known that internalization of microplastics significantly alters cell physiology, and is known to elicit an oxidative and inflammatory response in a dose-dependent manner (Dong *et al.*, 2020). By contrast, our approach develops cell sorting capabilities by creating layered substrates that can be physically detached from each other. The separation process is macroscopic (tweezers or sieve), in 2D and in 3D. In particular, collective effects based on conditioning by exogenous secretion or crowding effects can be readily controlled. The method here utilized collagen

Method	Principle/ Migration mode	Scale of isolation of live cells	Downstream assays demonstrated	Specialized method requirement	Ref.
Migration-based sorting after confined cell seeding (current work)	Spontaneous migration from original confined seeding zone onto (into) another substrate/ matrix (2D and 3D)	2D: 3×10^4 per well of six-well plate3D: 3×10^5 per well of six-well plate	Imaging, RT-qPCR, RNA-seq, functional assays (receptor clustering, T-cell killing)	Laser cutting	
Single-cellanalysis of motility and proteotype	Migration on polyacrylamide microchannels (2D)	≈100 cells per chip	Live imaging, in situ Western blot	Photolithography, microfluidics	Lin *et al.*, 2018
Motility behavioral screen	Separation based on phagocytosis of fluorescent particles when migrating of particle-coated surface (2D)	≈2000 cells per well of six-well plate	FACS, imaging	Fluorescent particles, FACS	Windler-Hart *et al.*, 2005
Single-cell migration chip	Capturing single cells migrating under chemotactic gradient using microfluidic device (2.5D?)	≈20 cells per chip	Imaging, RT-qPCR after proliferation	Lithography, microfluidics	Chen *et al.*, 2015
Microfluidic assay for quantification of cell invasion	Capturing cells that successfully migrate through narrow microfluidic channels (2.5D?)	≈100 cells per chip	Imaging, RT-qPCR, in vivo injection, RNA-seq	Lithography, microfluidics	Yankaskas *et al.*, 2019
Migration into Matrigel/growth factor–loaded needles	Selective isolation of cells that migrate into needles loaded with Matrigel, serum, and growth factors (3D)	≈1000 cells per needle	Imaging, RT-qPCR, cDNA microarray	Matrigel-filled microneedles	Wyckoff *et al.*, 2000; Patsialou *et al.*, 2012; Wang *et al.*, 2002, 2003, 2004

TABLE 1: Comparison of features of previously reported methods for migratory sorting of cells with the method demonstrated in the current work.

and HA, which are both abundant in most human tissues. Further, this approach can be expanded to other matrix molecules that can be added to bulk HA gels to select for cells that migrate better in their presence. Furthermore, the system can be adapted for chemotactic migration by incorporation of immobilized chemokines and growth factors in the outer HA hydrogel.

The 2D or 3D implementation of the assay does not involve any obstacle as in other chromatography approaches. It relies on the ability of the fastest cells to migrate from the initial colonies. Hence, the separation power of our technique depends on the collective behavior of the cells in the colony. It thus clearly selects cells that can escape from the initial dense mass of cancer cells. The spacer thickness and cell density can be varied for different cell types to ease the cell migration away from the colony. We found that for most cell lines an initial confinement on 300–500-μm-diameter pits (respectively, spheres) provide an adequate surface to perimeter ratio (respectively, volume to surface ratio) to allow migratory cells to explore the colony boundaries and enable them to emigrate. The sorting stringency can also be fine-tuned by modulating the time of migration. Hence, the sorting itself is a consequence of the device and of the initial population. We argue that the process of evasion from a dense cell mass, like in the current method, is a better recapitulation of tumor invasion where cells evade a dense solid tumor

than methods that isolate cells based on higher migration speed either on a sparsely seeded plastic surface or those based on single-cell migration in microfluidic channels.

Importantly, the 3D migration method opens avenues for migratory sorting of cells such as T-cells that do not migrate well on 2D substrates. Here we demonstrate the possibility of effectively sorting fast migrating cytotoxic T-cells using our method. Migratory sorting of T-cells is of very high relevance because of their need to traverse large distances in tissues before they attack their targets (Zhang *et al.*, 2019). Killing of cancer cells in the case of solid tumors involves the need to penetrate dense tissue before these cells can reach the core of the tumor. Strikingly, we report a strong correlation between migratory function and killing function of CTLs. It is beyond the scope of this article to establish the molecular reasons why these two distinct properties of CTLs (cell migration and killing function) are actually coupled. We can, however, speculate that the correlation can arise from the orchestration of these two distinct mechanisms by actin regulation (Serrador *et al.*, 1999; Gomez and Billadeau, 2008). The front-rear polarity development and persistence is largely governed by actin cytoskeleton dynamics (Angel *et al.*, 1999). The killing potential of T-cells is equivalently linked to the actin-based formation of immunological synapses (Dustin, 2007). Our method may thus be of great importance to sort cells

that would be able to migrate faster and better eliminate their target cancer cells in immunotherapeutic contexts.

Finally, the methods we propose here are easily scalable due to the simplicity of fabrication. The multilayer pits are fabricated on large PDMS sheets, drilled by a standard laser cutter and subsequently diced to the size of a six-well plate. The 3D version relies on a standard emulsification method. The combination of the power of the sorting method and the ease of implementation is key for a direct and wide adoption by other researchers and in clinical settings.

MATERIALS AND METHODS
Fabrication of layered-PDMS microwells
Four PDMS sheets of thickness 125 or 250 μm were layered over each other, and through holes of diameter 500 μm were created in it using a laser cutting machine as depicted in Figure 1. We tested several laser cutting machines for office work (e.g., engraving, sticker dicing), and most of them reached a sufficient resolution of 300 μm. The ash and debris from laser cutting were cleaned by sonication in an isopropanol/water mixture (1:1) for 10 mins. The device was rinsed several times with water, followed by drying using pressurized nitrogen. Finally, the PDMS layered device with through holes was layered over another PDMS sheet (125 μm). The large array was then cut into sizes as per experimental requirements. The microwell arrays were attached to tissue culture plates using Norland optical adhesive followed by UV curing.

Cell sorting using PDMS microwells
The PDMS microwells were UV sterilized and coated uniformly with fibronectin (50 μg/ml; Roche Lifescience). Because the fibronectin solution completely covers the microwells, it may be safe to assume that it will be adsorbed uniformly on the base as well as the sides of the wells. For cell seeding, 500 μl of cell suspension, ~(6–7) × 10^5 cells/ml, was added gently onto 8 × 8 wells/platform. Once the cells settle down inside the wells by gravity, the excess cells on the protecting layer are removed by giving a gentle wash to the PDMS device. The protecting layer is then peeled off with the help of sharp forceps to remove any cells on top of the device. Finally, enough media is added to completely submerge the device. The cells then migrate during the incubation period of 3–5 d. The collecting layer with the migrated cells can then be peeled off, as shown in Figure 1. The cells can thereafter be isolated by trypsinization from PDMS sheets and can then be cultured further or used for another analysis.

EMT scoring
Based on a previous study (Tan et al., 2014), EMT scoring was performed by analyzing gene expression data based on microarray analysis of a subset of cancer-related genes to score the different population in terms of their EMT status. To compute the EMT score in cell lines, a similar approach that was used in ssGSEA (Tan et al., 2014) was adopted. Empirical cumulative distribution function (ECDF) was estimated for epithelial and mesenchymal gene sets. The 2KS test was employed to compute the difference between the mesenchymal ECDF ($ECDF_{Mes}$) and the epithelial ECDF ($ECDF_{Epi}$). The 2KS score was then taken as the EMT score. A cell line with a positive EMT score exhibits a more "mesenchymal-like" phenotype, whereas a negative EMT score reflected a more "epithelial-like" phenotype.

Transcriptomic profiling of sorted cells
Migratory cells isolated using the 2D migration sorting assay were lysed using QIAzol. RNAs were purified using RNeasy mini kits in accordance with the manufacturer's protocol. Samples with RIN scores above 8, as determined by an Agilent RNA nano 600 kit/bioanalyzer, were sent to Bencos Research Solutions for RNA-sequencing and analysis. Briefly, a mRNA sequencing library was generated using a TruSeq stranded mRNA library preparation kit (illumina). The length and purity of the cDNA library was analyzed using an Agilent DNA1000 chip. The cDNA libraries were then paired-end sequenced using the HiSeq 2500. For RNA-seq analysis, reads were mapped to GRCh38 using STAR alignment (Dobin et al., 2013), and counted using HTSeq-count (Anders et al., 2015) before running DESeq2 (Love et al., 2014) and EdgeR (Robinson et al., 2010) for differential gene expression analysis (absolute log2-fold change [log2 FC] < 1 or [log2 FC] > 1, false discovery rate [FDR] < 0.05). GO analysis for differentially expressed genes was performed using Metascape (Zhou et al., 2019).

Ephrin clustering assay
Ephrin clustering assay was performed as reported previously (Ravasio et al., 2019). Briefly, nine chambers (3 × 3 mm) were formed by placing a silicon gasket on a clean, hydrophilic glass coverslip. Supported lipid bilayers with 96 mol% DOPC (Avanti Polar Lipids) and 4% DOGS-NTA-Ni (Avanti Polar Lipids) were then deposited using small unilamellar vesicle deposition. Polyhis-ephrinA1 labeled with Alexa 568 was then allowed to bind nitrilotri acetic acid (NTA) lipid moieties at saturating densities. The labeled bilayers were then washed. Cells were seeded on the wells and allowed to attach on the bilayer surface. The samples were fixed after 1 h and imaged using a fluorescence microscope.

Sorting of cancer cells using hierarchical hydrogels
For fabrication of collagen microgels, cells (either MDA MB 231 GFP or a mixture of MDA MB 231 GFP and MCF 7 at a ratio of 1:1) were suspended in cold neutralized bovine collagen solution (2.5 mg/ml; Thermo Fisher Scientific). This cell suspension was then added to prewarmed (37°C) mineral oil with 0.2% Span 80 while slowly stirring the oil using a magnetic stirrer. The emulsion was allowed to stir for 45 min. Thereafter, the emulsion was centrifuged at 1500 rpm for 5 min to separate microhydrogels from the oil phase. The pellet was washed three times with complete cell culture medium (DMEM with 10% fetal bovine serum) to remove traces of oil and surfactant. Finally, the gels were suspended in medium and cultured under regular cell culture conditions.

The fabricated microhydrogels after culture for 24 h were suspended in a hydrogel precursor solution containing HA-tyramine (5 mg/ml; LifeCore Biomedical), collagen (0.5 mg/ml), and horseradish peroxidase (2.5 U/ml) solution in phosphate buffered saline. Droplets of 100 μl of this suspension were then deposited in a 12-well plate. Thereafter, hydrogen peroxide was added to the droplets at a final concentration of 3 mM and mixed rapidly to enable crosslinking and gelation (<1 min). The gels were then incubated in complete cell culture medium at 37°C and 5% CO_2.

After 7 d of in vitro culture the samples were digested enzymatically using hyaluronidase (1 mg/ml in serum-free DMEM media; Sigma Aldrich) for 3 h at 37°C. This solution was then passed through a 40-μm cell strainer to separate single cells migrated out into bulk hydrogels from the cells retained in the microgels. The filtrate and the retentate containing the migrated and nonmigrated cells, respectively, were plated on regular cell culture dishes to enable culture and analysis of the two subpopulations.

T-cell sorting using collagen microbeads
T-cells were isolated from OT-1× Lifeact-EGFP mice spleens. To generate effector CD8+ T-cells, splenocytes were stimulated with

SIINFEKL peptide for 4 h in T-cell medium (TCM) and were then cultured with IL-2 for 6–7 d. For generation of collagen microgels 1×10^6 effector CTLs were suspended in neutralized ice-cold rat-tail collagen I solution (50 µl at 1.75–2 mg/ml; Corning). The addition of Alexa Fluor 647 succinimidyl ester (1 µl) allowed the visualization of the collagen particles during imaging. This cell suspension was then added to prewarmed (37°C) mineral oil with 0.2% Span 80 while slowly stirring the oil using a magnetic stirrer. The solution was stirred for 30 min allowing the formation of collagen microgels. Thereafter, the emulsion was centrifuged at 1500 rpm for 5 min to separate microhydrogels from the oil phase. The pellet was washed three times with TCM to discard traces of oil and surfactant. The collagen beads were incubated in 24-well plates for 2 h under regular culture conditions to allow T-cells to migrate out of the beads. The cell suspension that contained the microgels was passed through a 70-µm cell strainer separating the CTLs in suspension (migratory CTLs) from those retained in the microgels. Then the collagen microgels were treated with collagenase IV (0.5 mg/ml for 30 min; Sigma Aldrich) to isolate the nonmigrated cells (retained CTLs). To account for the effects of collagenase, unsorted CTLs (mix population with both migratory and retained cells) and the migratory CTL population were also treated with collagenase IV.

To validate our functional sorting, the isolated CTL populations were reembedded in collagen matrices and live imaged for 1 h to quantify migration parameters. Individual cells were then tracked in 3D and their average speeds and persistence ratios were measured (Galeano Niño et al., 2016).

Cytotoxic activity of T-cells

Cytotoxicity assays were performed using flow cytometry based on the ratio between live target and nontarget cells. A total number of 1×10^5 OT-1 T-cells was mixed with cognate (+SIINFEKL) and noncognate (–SIINFEKL) EL4 tumor cells (ATCC: TIB-39) at a ratio of 1:4:4. The cognate and noncognate cells were differentially labeled with cell tracker dyes and thus could be counted using flow cytometry analysis. Following exclusion of death cells (DAPI-ositive cells), the extent of reduction in the ratio of target to nontarget cells with respect to a control mix lacking T-cells was used as the measure of killing capacity of T-cells.

REFERENCES

Anders S, Pyl PT, Huber W (2015). HTSeq—a Python framework to work with high-throughput sequencing data. Bioinformatics 31, 166–169.

Angel M, Vicente-Manzanares M, Tejedor R, Serrador JM, Sánchez-Madrid F (1999). Rho GTPases control migration and polarization of adhesion molecules and cytoskeletal ERM components in T lymphocytes. Eur J Immunol 29, 3609–3620.

Ashby WJ, Zijlstra A (2012). Established and novel methods of interrogating two-dimensional cell migration. Integr Biol 4, 1338–1350.

Bai H, Li H, Li W, Gui T, Yang J, Cao D, Shen K (2015). The PI3K/AKT/mTOR pathway is a potential predictor of distinct invasive and migratory capacities in human ovarian cancer cell lines. Oncotarget 6, 25520.

Bajpai S, Mitchell MJ, King MR, Reinhart-King CA (2014). A microfluidic device to select for cells based on chemotactic phenotype. Technology 2, 101–105.

Chen H-C (2005). Boyden chamber assay. In: Cell Migration, New York: Springer, 15–22.

Chen Y-C, Allen SG, Ingram PN, Buckanovich R, Merajver SD, Yoon E (2015). Single-cell migration chip for chemotaxis-based microfluidic selection of heterogeneous cell populations. Sci Rep 5, 9980.

Chia S, Low J-L, Zhang X, Kwang X-L, Chong F-T, Sharma A, Bertrand D, Toh SY, Leong H-S, Thangavelu MT (2017). Phenotype-driven precision oncology as a guide for clinical decisions one patient at a time. Nat Commun 8, 1–12.

Cho D-H, Jo YK, Roh SA, Na Y-S, Kim TW, Jang SJ, Kim YS, Kim JC (2010). Upregulation of SPRR3 promotes colorectal tumorigenesis. Mol Med 16, 271–277.

Dobin A, Davis CA, Schlesinger F, Drenkow J, Zaleski C, Jha S, Batut P, Chaisson M, Gingeras TR (2013). STAR: ultrafast universal RNA-seq aligner. Bioinformatics 29, 15–21.

Dong C-D, Chen C-W, Chen Y-C, Chen H-H, Lee J-S, Lin C-H (2020). Polystyrene microplastic particles: in vitro pulmonary toxicity assessment. J Hazard Mater 385, 121575.

Dustin ML (2007). Cell adhesion molecules and actin cytoskeleton at immune synapses and kinapses. Curr Opin Cell Biol 19, 529–533.

Friedl P, Entschladen F, Conrad C, Niggemann B, Zänker KS (1998). CD4+ T lymphocytes migrating in threedimensional collagen lattices lack focal adhesions and utilize β1 integrin-independent strategies for polarization, interaction with collagen fibers and locomotion. Eur J Immunol 28, 2331–2343.

Galeano Niño JL, Kwan RY, Weninger W, Biro M (2016). Antigen-specific T cells fully conserve antitumour function following cryopreservation. Immunol Cell Biol 94, 411–418.

Gomez TS, Billadeau DD (2008). T cell activation and the cytoskeleton: you can't have one without the other. Adv Immunol 97, 1–64.

Jantscheff P, Terracciano L, Lowy A, Glatz-Krieger K, Grunert F, Micheel B, Brümmer J, Laffer U, Metzger U, Herrmann R (2003). Expression of CEACAM6 in resectable colorectal cancer: a factor of independent prognostic significance. J Clin Oncol 21, 3638–3646.

Jeong GS, Kwon GH, Kang AR, Jung BY, Park Y, Chung S, Lee S-H (2011). Microfluidic assay of endothelial cell migration in 3D interpenetrating polymer semi-network HA-Collagen hydrogel. Biomed Microdevices 13, 717–723.

Kramer N, Walzl A, Unger C, Rosner M, Krupitza G, Hengstschläger M, Dolznig H (2013). In vitro cell migration and invasion assays. Mutat Res/Rev Mutat Res 752, 10–24.

Krochmal M, Van Kessel KE, Zwarthoff EC, Belczacka I, Pejchinovski M, Vlahou A, Mischak H, Frantzi M (2019). Urinary peptide panel for prognostic assessment of bladder cancer relapse. Sci Rep 9, 1–10.

Lin J-MG, Kang C-C, Zhou Y, Huang H, Herr AE, Kumar S (2018). Linking invasive motility to protein expression in single tumor cells. Lab Chip 18, 371–384.

Love MI, Huber W, Anders S (2014). Moderated estimation of fold change and dispersion for RNA-seq data with DESeq2. Genome Biol 15, 550.

Lundgren K, Nordenskjöld B, Landberg G (2009). Hypoxia, Snail and incomplete epithelial–mesenchymal transition in breast cancer. Br J Cancer 101, 1769–1781.

Niño JLG, Tay SS, Tearle JL, Xie J, Govendir MA, Kempe D, Mazalo J, Drew AP, Colakoglu F, Kummerfeld SK (2020). The Lifeact-EGFP mouse is a translationally controlled fluorescent reporter of T cell activation. J Cell Sci 133, jcs238014.

Parker JJ, Canoll P, Niswander L, Kleinschmidt-DeMasters B, Foshay K, Waziri A (2018). Intratumoral heterogeneity of endogenous tumor cell invasive behavior in human glioblastoma. Sci Rep 8, 18002.

Patsialou A, Wang Y, Lin J, Whitney K, Goswami S, Kenny PA, Condeelis JS (2012). Selective gene-expression profiling of migratory tumor cells in vivo predicts clinical outcome in breast cancer patients. Breast Cancer Res 14, R139.

Qin H, Ni Y, Tong J, Zhao J, Zhou X, Cai W, Liang J, Yao X (2014). Elevated expression of CRYAB predicts unfavorable prognosis in non-small cell lung cancer. Med Oncol 31, 142.

Ravasio A, Zu Myaing M, Chia S, Arora A, Sathe A, Cao EY, Bertocchi C, Sharma A, Arasi B, Chung VY (2019). Single-cell analysis of EphA clustering phenotypes to probe cancer cell heterogeneity. BioRxiv 635102.

Robinson MD, McCarthy DJ, Smyth GK (2010). edgeR: a bioconductor package for differential expression analysis of digital gene expression data. Bioinformatics 26, 139–140.

Serrador JM, Nieto M, Sánchez-Madrid F (1999). Cytoskeletal rearrangement during migration and activation of T lymphocytes. Trends Cell Biol 9, 228–233.

Sharma A, Cao EY, Kumar V, Zhang X, Leong HS, Wong AML, Ramakrishnan N, Hakimullah M, Teo HMV, Chong FT (2018). Longitudinal single-cell RNA sequencing of patient-derived primary cells reveals drug-induced infidelity in stem cell hierarchy. Nat Commun 9, 1–17.

Tan TZ, Miow QH, Miki Y, Noda T, Mori S, Huang RYJ, Thiery JP (2014). Epithelial-mesenchymal transition spectrum quantification and its

efficacy in deciphering survival and drug responses of cancer patients. EMBO Mol Med 6, 1279–1293.

Wang W, Goswami S, Lapidus K, Wells AL, Wyckoff JB, Sahai E, Singer RH, Segall JE, Condeelis JS (2004). Identification and testing of a gene expression signature of invasive carcinoma cells within primary mammary tumors. Cancer Res 64, 8585–8594.

Wang W, Wyckoff JB, Frohlich VC, Oleynikov Y, Hüttelmaier S, Zavadil J, Cermak L, Bottinger EP, Singer RH, White JG (2002). Single cell behavior in metastatic primary mammary tumors correlated with gene expression patterns revealed by molecular profiling. Cancer Res 62, 6278–6288.

Wang W, Wyckoff JB, Wang Y, Bottinger EP, Segall JE, Condeelis JS (2003). Gene expression analysis on small numbers of invasive cells collected by chemotaxis from primary mammary tumors of the mouse. BMC Biotechnol 3, 13.

Windler-Hart SL, Chen KY, Chenn A (2005). A cell behavior screen: identification, sorting, and enrichment of cells based on motility. BMC Cell Biol 6, 14.

Wyckoff JB, Segall JE, Condeelis JS (2000). The collection of the motile population of cells from a living tumor. Cancer Res 60, 5401–5404.

Yankaskas CL, Thompson KN, Paul CD, Vitolo MI, Mistriotis P, Mahendra A, Bajpai VK, Shea DJ, Manto KM, Chai AC (2019). A microfluidic assay for the quantification of the metastatic propensity of breast cancer specimens. Nat Biomed Eng 3, 452–465.

Zhang J, Endres S, Kobold S (2019). Enhancing tumor T cell infiltration to enable cancer immunotherapy. Immunotherapy 11, 201–213.

Zhou Y, Zhou B, Pache L, Chang M, Khodabakhshi AH, Tanaseichuk O, Benner C, Chanda SK (2019). Metascape provides a biologist-oriented resource for the analysis of systems-level datasets. Nat Commun 10, 1–10.